Resource

Cell Reports

A Cell-Signaling Network Temporally Resolves Specific versus Promiscuous Phosphorylation

Graphical Abstract

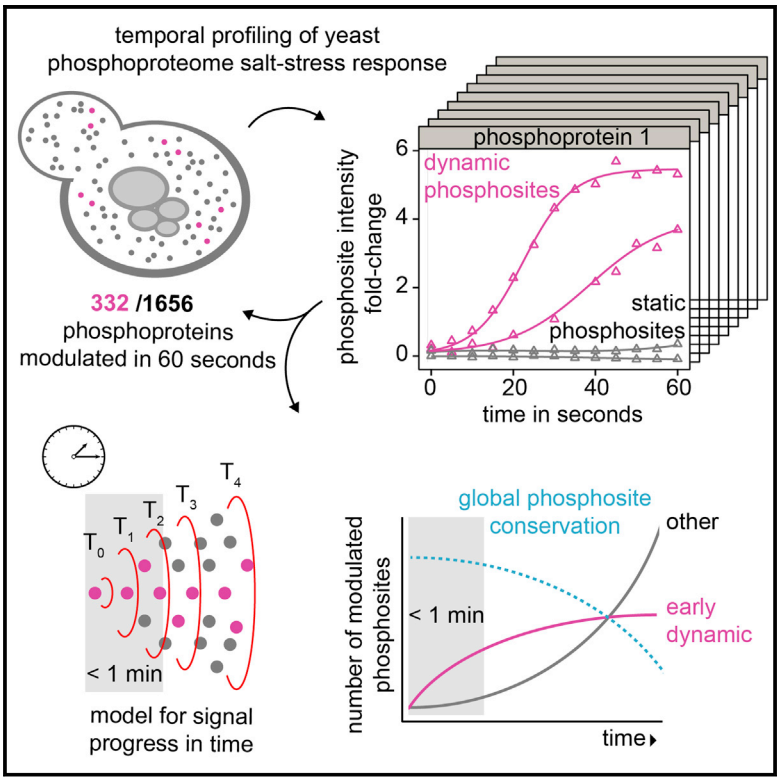

Authors

Evgeny Kanshin,
Louis-Philippe Bergeron-Sandoval, ...,
Pierre Thibault, Stephen W. Michnick

Correspondence

pierre.thibault@umontreal.ca (P.T.),
stephen.michnick@umontreal.ca
(S.W.M.)

In Brief

Kanshin et al. report that conserved and putatively functional kinase- or phosphatase-substrate interactions in the high-osmolarity glycerol (HOG) response occur more rapidly than promiscuous interactions. They provide a rich data set of dynamic phosphosites that may be implicated in the regulation of the cell cycle, cytoskeletal dynamics, and morphogenesis.

Highlights

- A strategy for phosphoproteomics at high temporal resolution and coverage
- The HOG-signaling network involves 25% of the kinome and 10% of phosphatases
- Changes in functional phosphorylation occur more rapidly than promiscuous events
- Many potentially regulatory phosphosites in cytoskeletal proteins are reported

Kanshin et al., 2015, Cell Reports *10*, 1202–1214
February 24, 2015 ©2015 The Authors
http://dx.doi.org/10.1016/j.celrep.2015.01.052

OPEN ACCESS
CellPress

Cell Reports
Resource

A Cell-Signaling Network Temporally Resolves Specific versus Promiscuous Phosphorylation

Evgeny Kanshin,[1,4,5] Louis-Philippe Bergeron-Sandoval,[1,5] S. Sinan Isik,[1] Pierre Thibault,[1,2,4,*] and Stephen W. Michnick[1,3,*]

[1]Département de Biochimie, Université de Montréal, C.P. 6128, Succursale centre-ville, Montréal, QC H3C 3J7, Canada
[2]Département de Chimie, Université de Montréal, C.P. 6128, Succursale centre-ville, Montréal, QC H3C 3J7, Canada
[3]Centre Robert-Cedergren, Bio-Informatique et Génomique, Université de Montréal, C.P. 6128, Succursale centre-ville, Montréal, QC H3C 3J7, Canada
[4]Institute for Research in Immunology and Cancer, Université de Montréal, C.P. 6128, Succursale centre-ville, Montréal, QC H3C 3J7, Canada
[5]Co-first author
*Correspondence: pierre.thibault@umontreal.ca (P.T.), stephen.michnick@umontreal.ca (S.W.M.)
http://dx.doi.org/10.1016/j.celrep.2015.01.052

SUMMARY

If specific and functional kinase- or phosphatase-substrate interactions are optimized for binding compared to promiscuous interactions, then changes in phosphorylation should occur faster on functional versus promiscuous substrates. To test this hypothesis, we designed a high temporal resolution global phosphoproteomics protocol to study the high-osmolarity glycerol (HOG) response in the budding yeast *Saccharomyces cerevisiae*. The method provides accurate, stimulus-specific measurement of phosphoproteome changes, quantitative analysis of phosphodynamics at sub-minute temporal resolution, and detection of more phosphosites. Rates of evolution of dynamic phosphosites were comparable to those of known functional phosphosites and significantly lower than static or longer-time-frame dynamic phosphosites. Kinetic profile analyses indicated that putatively functional kinase- or phosphatase-substrate interactions occur more rapidly, within 60 s, than promiscuous interactions. Finally, we report many changes in phosphorylation of proteins implicated in cytoskeletal and mitotic spindle dynamics that may underlie regulation of cell cycle and morphogenesis.

INTRODUCTION

Signaling networks have evolved to respond to distinct environmental stimuli with coherent and specific responses. Yet recent evidence suggests that protein kinases, the major signaling enzymes in the cell, form a highly connected and perhaps irreducibly complex network (Bodenmiller et al., 2010; Breitkreutz et al., 2010). We have argued that complexity of the kinase network may have evolved to integrate and compare multiple signals, resulting in main and complementary responses to stimuli (Levy et al., 2010). Such a network could also generate promiscuous phosphorylation that has no functional consequence but confounds our understanding of the signaling response (Figure 1A; Landry et al., 2009; Levy et al., 2012).

It is generally viewed that signaling networks have evolved so that kinase- or phosphatase-substrate interactions are made most efficient by optimization of enzyme binding and specificity for substrate recognition sequences and structural organization through domain, adaptor, or scaffold protein binding (Bhattacharyya et al., 2006; Scott and Pawson, 2009; Zheng et al., 2013). We hypothesize that functional phosphorylation of specific substrates occurs rapidly following stimulation but that promiscuous phosphorylation takes place more slowly, following random encounters with neighboring proteins (Figure 1B). Therefore, capturing early signaling (phosphorylation or dephosphorylation) immediately after cell stimuli could facilitate the detection of stimulus-specific phosphorylation.

To test this hypothesis, we chose the high-osmolarity glycerol (HOG) response pathway of the budding yeast *Saccharomyces cerevisiae* and performed rapid (5-s resolution) phosphoproteomics analyses to yield unprecedented profiling of HOG signaling (Chen and Thorner, 2007; Gustin et al., 1998; Saito and Posas, 2012). We chose to study this response because the signaling pathways are very well characterized and temporal responses have been studied in detail (Hersen et al., 2008; Muzzey et al., 2009; Saito and Posas, 2012). In addition, cell-to-cell variation of the response is very low so that dynamics of phosphorylation likely reflect responses of all cells in the whole population studied and not some subpopulation.

RESULTS

Dynamic Phosphoproteomics at Sub-minute Temporal Resolution

Common sample preparation protocols used in phosphoproteomics are not generally suited to the profiling of rapid signaling events because cell harvesting typically requires 5–15 min due to centrifugation and cell pellet washing steps. These steps can impart changes to the phosphoproteome that arise from both the stimulus of interest and the sample collection method. Thus, to assure that measured changes in the phosphoproteome are

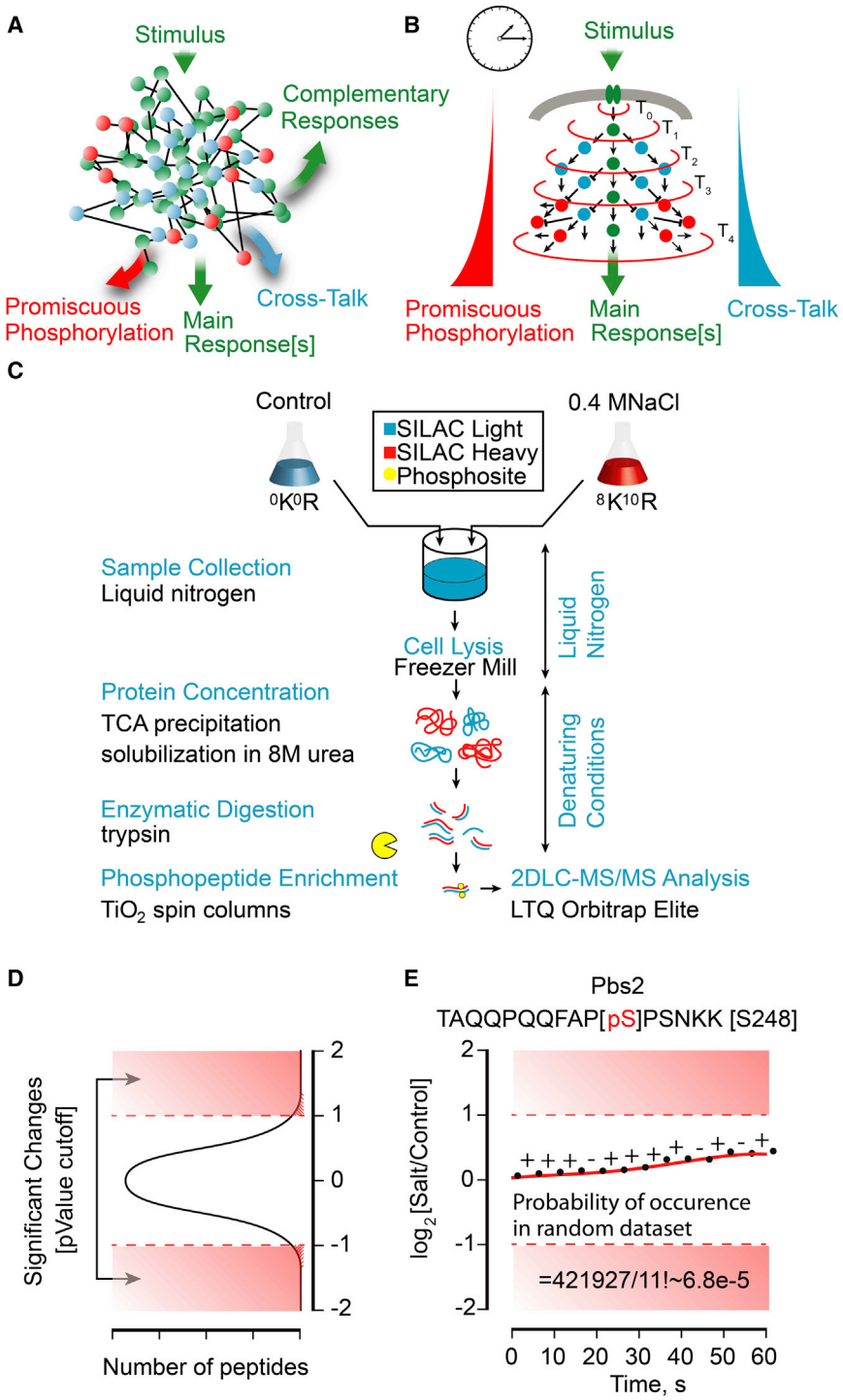

Figure 1. The Origins of Complexity in Signaling Networks

(A) Signaling networks composed of kinases and phosphatases (green and blue dots) may be highly connected (dark lines), resulting in main and complementary responses to stimuli. Signaling that has no consequences could arise due to promiscuous phosphorylation that masks simple pathways (red dots).

(B) We hypothesize that stimulus-specific signaling may occur faster than promiscuous signaling.

(C) Experimental workflow to study phosphoproteome dynamics at high temporal resolution. Samples are collected by flash freezing yeast cultures in liquid nitrogen to preserve phosphorylation status.

(D–E) A pattern- and fold-change-based analysis of high-resolution phosphorylation kinetic profiles. (D) Common data analysis workflows use the distribution of fold changes for detected phosphopeptides in order to define regulated phosphosites. (E) To detect changes in phosphorylation with small fold change value, such as Pbs2 Ser248, a pattern-based analysis with ± signatures of the kinetic profiles (independent of absolute fold change) was used to assign significance of individual low-amplitude traces.

See also Figure S1 and Table S1.

due only to the stimulus applied and to facilitate the dynamic studies at sub-minute temporal resolution, we devised a new sample-collection technique (Figure 1C). Yeast cells grown in media containing either light (control) or heavy (0.4 M NaCl) isotopic forms of arginine and lysine were pooled together in liquid nitrogen to prevent any protein degradation and further activity of kinases and phosphatases. Frozen cell cultures from 13 time points ranging from 0 to 60 s (at 5-s intervals) were finely ground under liquid nitrogen; TCA-precipitated proteins were resolubilized in denaturing urea buffer and digested with trypsin. Importantly, we could perform protein extraction with no intermediate washing steps. Consequently, cells were not exposed to perturbing wash conditions that could cause changes in the phosphoproteome. Phosphopeptides were enriched on TiO_2 resin prior to offline separation on SCX spin columns and LC-MS/MS analyses (Supplemental Experimental Procedures; Harsha et al., 2008; Ong et al., 2002; Ong and Mann, 2006).

We collected temporal profiles for 5,453 phosphopeptides on 1,656 proteins with a false discovery rate (FDR) less than 1% at both peptide and protein levels. These profiles corresponded to phosphopeptides quantified in at least 10 of 13 time points with an average phosphosite localization confidence greater than 0.75 (Figures S1A and S1B; Table S1). We identified 596 phosphopeptides from 332 proteins that showed distinct continuous changes in phosphorylation with time (increases or decreases; Table S2). Abundances of the remaining phosphopeptides did not change with time (henceforth, they are defined as containing "static" phosphosites). All the dynamic and static phosphosite temporal profiles can be displayed using an R script (Data S1). The high

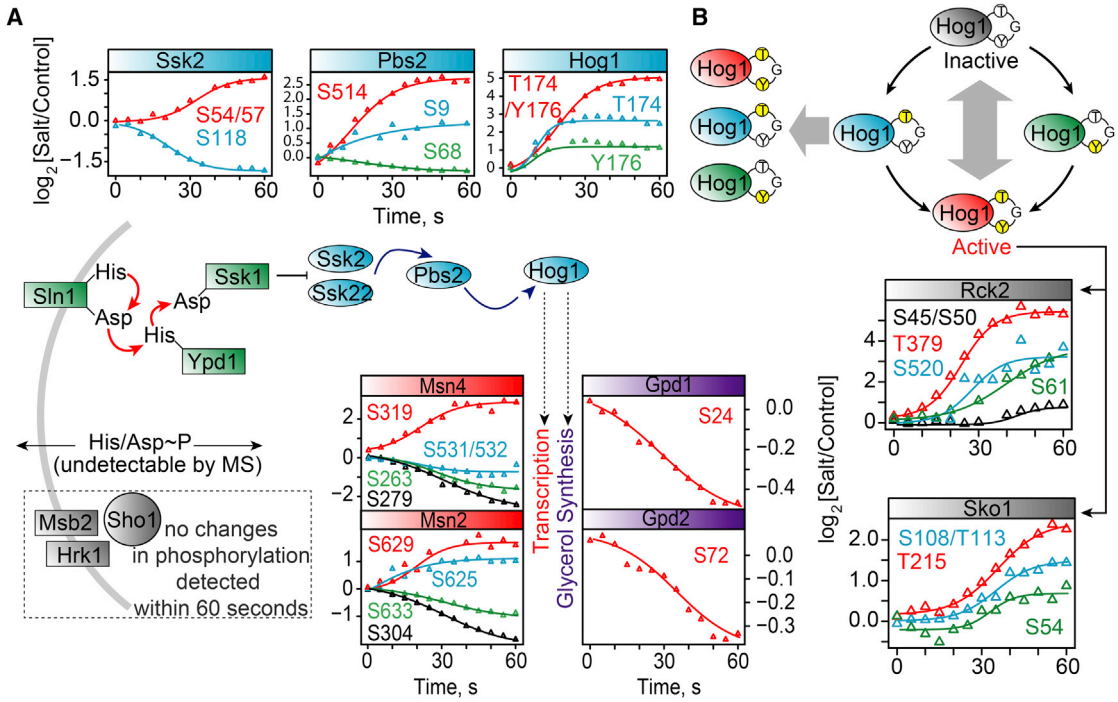

Figure 2. Dynamic Phosphorylation within the Canonical HOG Pathway

(A) Changes on MAPK (Hog1), MAPKK (Pbs2), and MAPKKK (Ssk2) were detected within the canonical yeast HOG pathway. We were unable to detect dynamic phosphorylation upstream of Ssk2 because of the labile nature of phosphorylation on Asp and His residues.

(B) Schematic representation of the observed dynamic double phosphorylation of Hog1 and subsequent phosphosite kinetics profiles in Hog1 substrates Rck2 and Sko1.

See also Figure S2.

temporal resolution of changes in phosphorylation obtained in this study enabled us to use a pattern-based algorithm to identify 99 additional regulated phosphosites, including for those with kinetic profiles of low amplitude that would remain undetected by conventional quantitative phosphoproteomic approaches (Supplemental Experimental Procedures; Figures 1D, 1E, S1C, and S1D–S1H; Willbrand et al., 2005). The reproducibility of sample processing and data analysis was confirmed through independent experiments (Figures S1E–S1G).

Recapitulation of the Canonical HOG Pathway

We first examined signaling within the canonical HOG-signaling pathway, generally depicted as cascades of phosphorylation-activation steps (Figure 2A; Saito and Posas, 2012). The canonical HOG pathway has two branches, emanating from cell-surface osmo-receptors Sho1 and Sln1, both of which converge upon the scaffold protein-MAPKK Pbs2 and ultimately the MAPK Hog1. Early responses include cell shrinkage due to exit of water within seconds and slower nuclear translocation of Hog1 within several minutes (Muzzey et al., 2009). Simultaneously, the cell cycle arrests, channels controlling glycerol, and other osmolytes are affected and gene transcription is modulated, ultimately resulting in adaptation to changed osmolarity.

Our rapid sample preparation strategy resulted in accurate observation of dynamic phosphorylation of components of the HOG response pathway (Figure 2A). For example, we obtained distinct profiles for both monophosphorylated forms of Hog1 on its activation loop (T174/Y176; Figure 2B), observing greater than 30-fold increase within 40 s following stimulation.

We did not observe changes in the Sln1 branch upstream of Ssk2. This is predictable because this branch is affected through a two-component histidine-aspartate phosphorelay (Figure 2A). The lability of these phosphosites prevents their detection under the conditions that we performed our experiments. We also did not observe rapid changes in phosphorylation of substrates for the Sho1 branch. It is possible that these sites are phosphorylated at low stoichiometry or, alternatively, that the Sho1 branch is activated on a different timescale (Macia et al., 2009). For instance, changes in phosphorylation of both PAK-like kinases Ste20 (T203, S206, and S169) and Cla4 (S367) occurred more slowly than Hog1 phosphorylation (Table S2), suggesting that these result from later feedback phosphorylation of these proteins.

The quality of the kinetic profiles is reflected by the continuity of increasing or decreasing sequential data values between time points that we observe (Figures 2 and 3). This continuity reflects the fact that, when cells are immediately frozen in liquid nitrogen, no spurious changes in phosphorylation may occur.

Anticipatory Signaling Downstream of the Canonical HOG Pathway

We observed dynamic changes in phosphorylation for a number of reported substrates of Hog1, including transcription factors

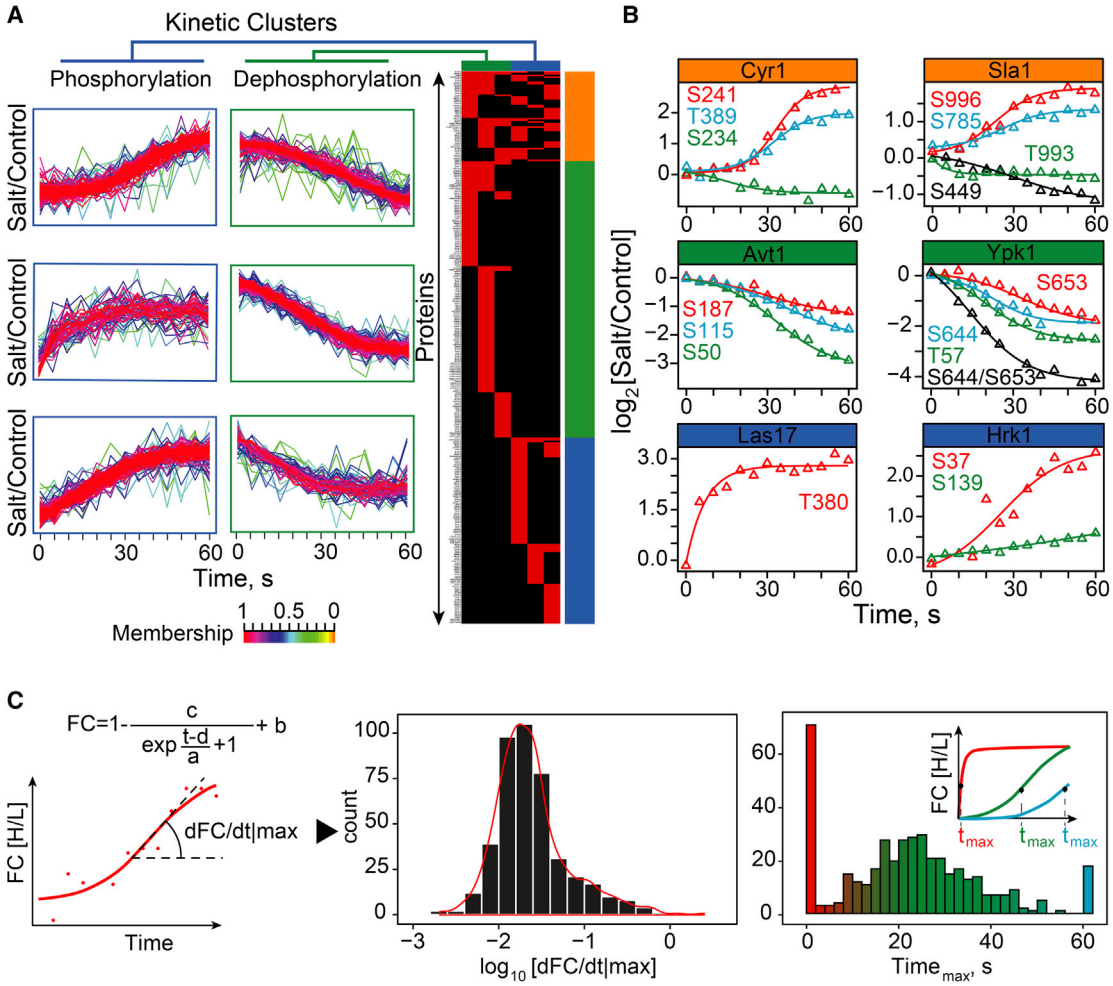

Figure 3. Kinetic Analysis of Signaling Response

(A) Kinetic profiles can be clustered into six types (left). The cluster membership of the kinetic profiles is color coded according to the scale shown below the clusters. The 596 dynamic phosphosites identified fall into three distinct protein groups: phosphorylated (blue box); dephosphorylated (green box); or both on distinct sites of the same protein (orange box). These dynamic sites are contained within 332 proteins displayed in the right panel heatmap according to site-associated kinetic cluster groups.

(B) Examples of dynamic phosphorylation sites from each group are presented in the left panels.

(C) Fitting of kinetic profiles to a birth-death model enabled the extraction of maximum rates of fold change (dFC/dt_{max}; right) and times at which the maximum rate is achieved (t_{max}). The distribution of rates (dFC/dt_{max}) from 596 dynamic sites on a $\log_{10}$ scale shows that 68% of rates (dFC/dt_{max}) fall within one order of magnitude. Profile fitting demonstrated that 72.5% of profiles are sigmoidal in shape (see Figure S3) and reach t_{max} within a time window of 60 s (green bars in the right panel and green trace in the right panel insert). No sigmoidal-like profiles reached t_{max} at 0 or 60 s (respectively represented as red and blue bars and traces in the right panel and insert) in contrast to exponential or linear-like profiles.

See also Figure S3 and Table S2.

Sko1, Msn2, and Msn4 and Rck2 kinase, as well as glycerol response proteins Gpd1 and Gpd2 (Bilsland-Marchesan et al., 2000; Lee et al., 2012; Proft and Struhl, 2002; Teige et al., 2001; Vaga et al., 2014; Figure 2). Surprisingly, we noted a rapid dephosphorylation of the kinase Ssk2 at residue S118 and phosphorylation on residues S54 and S57 (Figure 2A). Previous reports indicated that Ssk2 concentrates in the bud neck and forms a complex with actin during osmotic stress, where it promotes actin cytoskeleton recovery through the reestablishment of osmotic balance (Bettinger et al., 2007; Yuzyuk and Amberg, 2003; Yuzyuk et al., 2002). However, these events should occur during the later adaptive period of HOG response and may involve different sites than those identified here. The dynamic phosphosites we observed may be anticipatory signals, perhaps involved in the re-localization of Ssk2 to the bud neck prior to activation during the adaptive phase.

We also observed complex phosphorylation patterns for the general stress transcription factors Msn2 and Msn4 (Figure 2A; Reiter et al., 2013). Hyperosmotic stress was previously shown to result in a short-lived dephosphorylation of Msn2 on at least six serine residues (S194, S201, S288, S304, S451, and S633), two of which (S304 and S633) were observed in this study.

Phosphorylation of Msn2 was also detected on PKA consensus sites (S625/S629) located in the nuclear localization sequence (NLS) and associated with the sequestration of Msn2 to the nucleus to favor its association with chromatin (Reiter et al., 2013). Early phosphorylation of these sites could be involved in the re-equilibration of active Hog1 to the nucleus as suggested previously (Mattison and Ota, 2000; Reiser et al., 1999; Rep et al., 1999).

Interestingly, we observed a gradual dephosphorylation of Fps1 on residues 172, 175, 181, and 185 proximal to a putative MAPK-docking site (D motif; Sharrocks et al., 2000) within this region (residues 176–187; Figure S2). It was recently reported that, upon osmotic shock, Hog1 is recruited to a MAPK-docking site within the N-terminal domain of Fps1 and phosphorylates a redundant pair of regulators, Rgc1 and Rgc2, to induce their eviction from the C-terminal region of Fps1, which in turn causes closure of the Fps1 channel (Figure S2A; Lee et al., 2013). Phosphorylation/dephosphorylation of serines 172, 175, 181, and 185 could act as a regulatory switch to modulate docking of Hog1 via its interaction with neighboring arginine residues of the Fps1 D motif (Figure S2B). Accordingly, dephosphorylation of N-terminal residues of Fps1 would favor docking of Hog1 to the D-motif, which is used as a platform to phosphorylate Rgc1/2. Consistent with this proposal, we also observed an increase in phosphorylation of residues 21, 975, 1,046, 1,048, and 1,059 of Rgc1 upon osmotic shock (Figure S2C).

Global Dynamic Properties of the HOG Signaling Response

We next examined global dynamic properties of the HOG signaling response. We used fuzzy c-means clustering to group our phosphosites into six distinct clusters according to the shape of their kinetic profiles (cluster membership > 0.5; Supplemental Experimental Procedures; Table S2). Analysis of the distribution of dynamic phosphosites on the corresponding proteins revealed three distinct protein groups that were either phosphorylated (200 profiles), dephosphorylated (183 profiles), or displayed both behaviors (58 profiles; Figure 3A). The last group, which includes the proteins Cyr1 and Sla1 (Figure 3B), is the most interesting because it contains proteins that could interact with at least one kinase and phosphatase or be phosphorylated on multiple sites by the same kinase.

To access the temporal nature of the responses, we empirically fit profiles to a simple birth-death model and extracted two parameters: the maximum rate of fold change corresponding to an increase or decrease in phosphorylation (dFC/dt_{max}) and the time at which the maximum rate is observed (t_{max}; Supplemental Experimental Procedures; Figure 3C; Table S2).

The temporal resolution we achieved in this study enabled us to discern key features of the dynamic responses. Notably, 72.5% of dynamic profiles are sigmoidal in shape (Figure S3), and most profiles approach their maxima (or minima) within 60 s (Figure 3C, right). The latter suggest that either the HOG response reaches its maximum within 60 s or, if there are later responses, they occur on a different timescale than studied here. The sigmoidal responses are interesting in that they resemble low-pass-filter outputs that block high frequency and random short-period noise of extracellular or intracellular origins. Specifically, the delay in response of a sigmoid curve assures that any random, short-duration signals will not induce a response. Furthermore, the sigmoid response assures that sequential steps in signal processing occur at rates that are optimal for the reactions in a given pathway (Tay et al., 2010). Indeed, our results are consistent with observed responses of the HOG pathway as a function of the frequency of oscillating stimuli (Hersen et al., 2008; Muzzey et al., 2009).

We also observed that the range of maximum-rate fold change is tapered compared to a normal distribution and 68.3% of these rates fall within one order of magnitude (Figure 3C, middle). This is a curious result, because one might expect reaction rates of kinases and phosphatases to have a broad distribution due to differences in intrinsic activity, substrate abundances, their subcellular localizations, structures, and enzyme recognition sequences (though note that we do not measure changes in absolute rates here). Such a narrow range of rates could be favored by organization of enzymes and substrates into complexes or physical localization to specific cellular compartments (Bhattacharyya et al., 2006; Scott and Pawson, 2009; Zheng et al., 2013).

Dynamic Phosphorylation Suggests a Dense Kinase-Phosphatase Network

At the outset, we hypothesized that the complexity of signaling events could arise from the propagation of signaling through a highly connected kinase-phosphatase network, resulting in main, complementary, and promiscuous responses (Figure 1A). We did observe a constant increase in width of fold change distributions with time (Figure S4A) and an almost 9-fold increase in the number of affected phosphosites during the first minute following osmotic shock (Figure 4A). The speed of the signal propagation is very rapid with 84 phosphosites changing in the first 5 s, whereas the complexity of the response increases concurrently. We further predict that, if there is a complex kinase-phosphatase network, many of these enzymes undergo changes in phosphorylation early in response to stimulus. We observed that 25% (34/129) of all kinases and 10% (3/30) of all phosphatases had dynamic phosphosites changing within 60 s following stimulation and 28 of the kinases and the three phosphatases are known to have at least one interaction with another kinase or phosphatase (Figure 4B; Table S2). Thus, it is possible that the combinatorial explosion of phosphorylation events we observe is due to rapid changes of enzyme activities in a highly connected kinase-phosphatase network.

If the changes in phosphorylation of the kinases or phosphatases described above resulted in either activation or inactivation of these enzymes, then we could predict that regulated phosphosites are surrounded by peptide motifs that are recognized by these enzymes. To test this hypothesis, we performed two independent tests: one to predict kinases that could phosphorylate the observed phosphosites using NetworKIN (Figure S4B) and a second test for overrepresentation of linear peptide motifs surrounding dynamic phosphosites using MotifX (Chou and Schwartz, 2011; Linding et al., 2007; Schwartz and Gygi, 2005). We found overrepresentation of peptide motifs for those with basic residues in p-2 to p-5 positions relative to the phosphosite (Figure 4C, left). Furthermore, 13 of the 34 kinases that showed dynamic phosphorylation changes have been

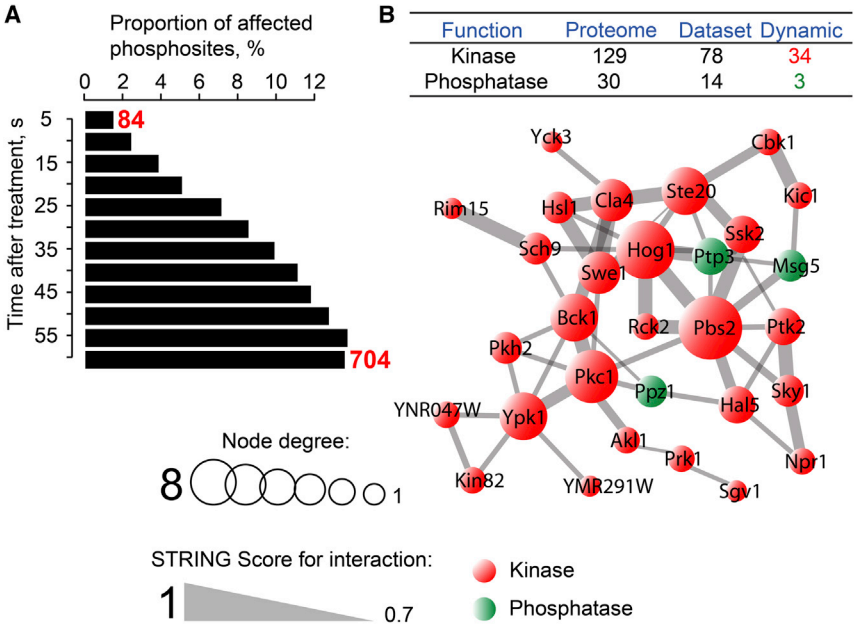

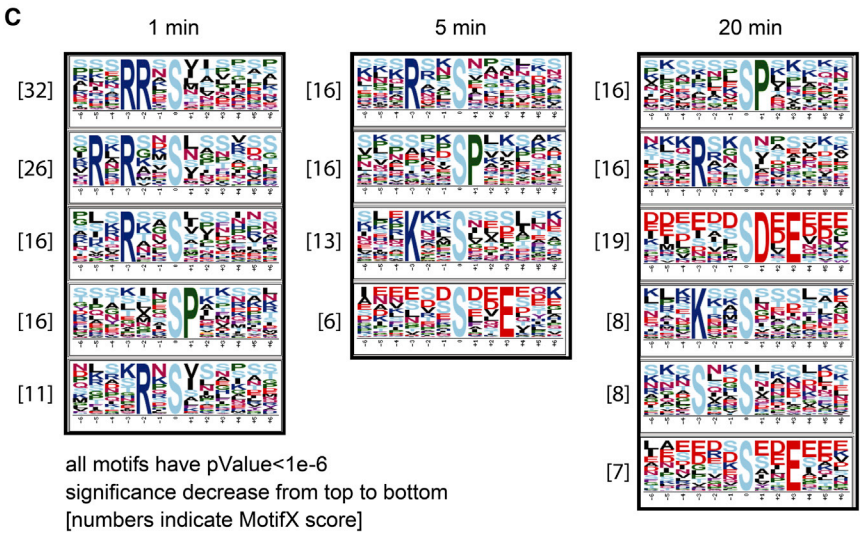

Figure 4. Temporal Complexity of the Kinase-Phosphatase Network and Relationships with Dynamic Substrates

(A) The number of phosphosites that undergo a significant fold change increased with time (84 to 704 sites from 5 to 60 s after osmotic shock).

(B) The HOG kinase-phosphatase network appears to be complex. Network based on known kinase-phosphatase relationships (from STRING database; http://string-db.org/).

(C) Overrepresented linear motifs in our data were detected with MotifX (Chou and Schwartz, 2011; Schwartz and Gygi, 2005). We used default settings (min. occurrences = 20; significance = 0.000001) and SGD proteome as background. As a result, we obtained different motifs among phosphosites regulated within 1, 5, and 20 min upon osmotic shock.

See also Figure S4 and Table S2.

experimentally demonstrated to recognize such basic peptide motifs (Mok et al., 2010). NetworKIN showed enrichment for basophilic PKA and PAK kinases (PAKA), consistent with the MotifX search results (Figure S4B). We can also conservatively predict that at least 18 of the kinases likely recognize peptides with basic residues in the p-2 to -5 positions based on their membership to the AGC family of protein kinases (Table S2; Manning et al., 2002).

Phosphorylation of sites with prolines at p+1 are the most expected, assuming that the canonical HOG response involves activation of MAP kinases. Such motifs are indeed enriched in our 1 min data, though not dominant. Some phosphorylation motifs at 5 and 20 min (Soufi et al., 2009) are acidic across the entire motif (Figure 4C, middle and right) and could reflect the activation of acidophilic kinases of the casein kinase 2 (CK2) family at later time points.

Dynamic Phosphosites Are More Conserved Than Static Phosphosites

We previously proposed that the apparent complexity of signaling networks could be partially due to non-functional promiscuous phosphorylation (Landry et al., 2009; Levy et al., 2012). We proposed here that rapidly phosphorylated phosphosites (dynamic sites) would be more likely functional and therefore more conserved than phosphosites that are phosphorylated more slowly (static sites), some of which may accumulate over very long (greater than one cell cycle) time frames. We found that, on average, dynamic sites are significantly more conserved than static sites ($p < 0.005$) whereas no significant differences were observed in a study performed at 5 and 20 min following osmotic shock (Figure 5A; Soufi et al., 2009). Furthermore, the evolutionary rates of our dynamic sites were similar to those of literature-curated functional sites ($p = 0.3420$; Nguyen Ba and Moses, 2010). Thus, it appears that, in the initial response to osmotic shock, there is an enrichment of functional phosphosites in the dynamic compared to static phosphosites.

Conserved Phosphosites of Pathway-Specific Proteins Are Functional

Having compared functional to dynamic and static site conservation, we now did the reverse, selecting conserved known sites and sites we discovered for their potential functional relevance. To do this, we chose proteins from two pathways, including proteins from the HOG response (Hog1, Rck2, and Gpd1) and from

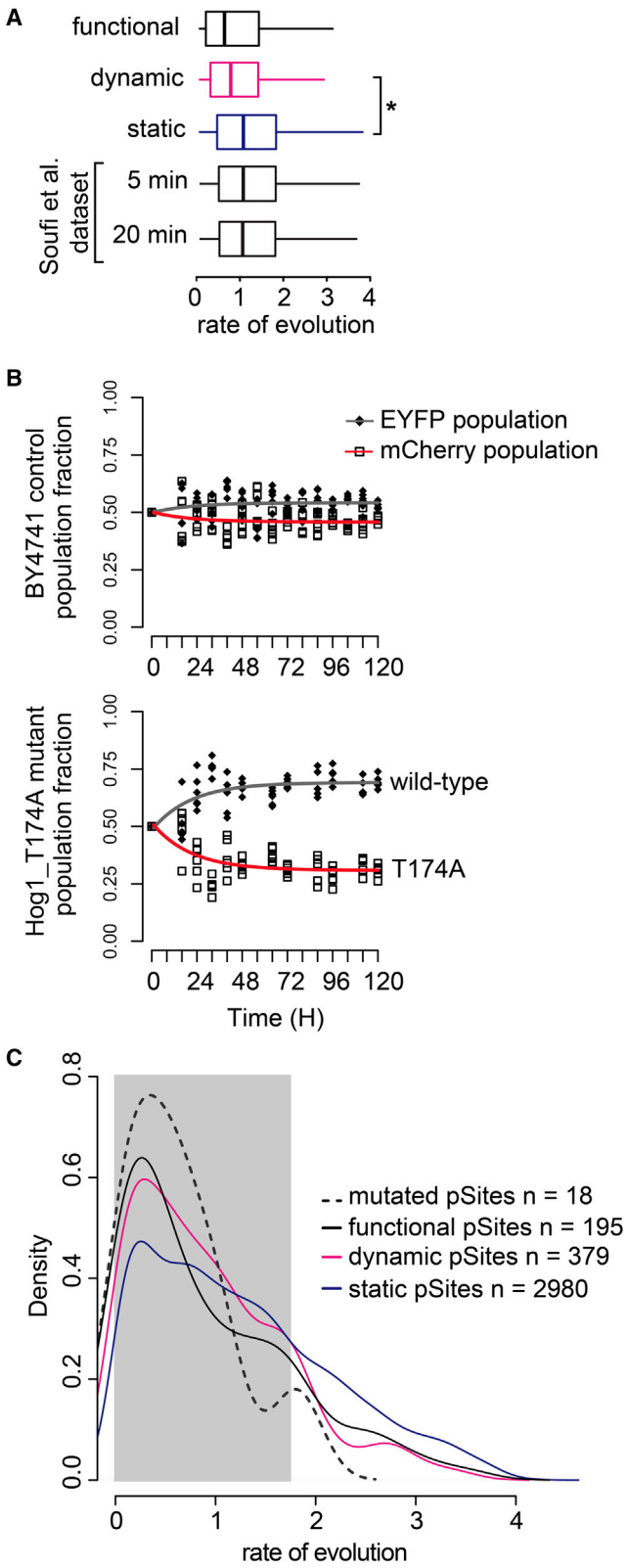

Figure 5. Dynamic Phosphosites of the HOG Responses Are Globally More Conserved Than Static Phosphosites, and Conserved Phosphosites Affect Cell Fitness

(A) The comparison of rates of evolution shows that dynamic phosphorylation sites (n = 474) are more conserved than static ones (n = 3751; p = 0.0014) but do not differ from known functional phosphorylation sites (n = 249). Only dynamic and static sites with a single modified residue were considered for this analysis.

(B) Population fractions of phospho-null Hog1 T174A mutant versus Hog1 wild-type strains (bottom graph) were determined in competition-growth assays using specific fluorescent reporters for the respective mutant (mCherry; empty squares and red curve) and the wild-type (EYFP; dark diamonds and gray curve) strains. Control assay was performed with strains of BY4741 expressing either mCherry or EYFP and grown in competition with each other to access normal population fluctuations (upper graph).

(C) The density distribution of phospho-null mutants (dashed), functional (black), dynamic (magenta), and static (blue) phosphosites rates of evolution shows the proportion of conserved sites in the respective populations (rate of evolution cutoff = 1.8; light gray area). Seventy-two percent of the conserved phosphosites we sampled from our data set are functional (13/18; binomial test p = 0.0481), and their distribution is showed with the dashed black line. See also Figure S5.

complementary changes observed in actin and tubulin cytoskeletal proteins (Bud6, Bim1, Syp1, and Sla1). We performed competition-growth assays to determine the fitness of dynamic and static phospho-null mutants (serine, threonine, or tyrosine to alanine mutations) compared to their respective wild-type proteins (Figures 5B and S5). For assessment of fitness under different conditions, we selected 13 dynamic and five static sites that are all conserved, with a rate of evolution below 1.8 (Figures 5C and S5; Landry et al., 2009; Levy et al., 2012).

The mutants were all expressed from plasmids encoding the ORF of each gene flanked by native promoters and terminators (Ho et al., 2009). Each phospho-null strain was also transformed with a plasmid coding for mCherry monomeric RFP and the wild-type strains with a plasmid coding for EYFP (Supplemental Experimental Procedures). Growth-competition assays were performed starting from equal numbers of mutant and wild-type cells. Competition cultures were maintained in exponential growth phase for 5 days, and the significant population fraction amplitude changes were determined by fluorescence spectroscopy (Figures 5B and S5). Competition assays were performed in low-fluorescence medium (LFM) or LFM plus 1 M NaCl to detect phosphosites that have impact on fitness in different cellular context.

We compared the distribution of the mutated, functional, dynamic, and static sites versus rates of evolution (Figure 5C). Within the window of conserved sites (rate of evolution < 1.8), we observed that the distribution of the phospho-null mutants was similar to those of the functional and dynamic sites, with a high proportion (0.72; binomial test p = 0.0481) of these sites that showed a fitness effect.

HOG Modulates Cytoskeletal and Morphogenic Pathways

We predict that a complex kinase-phosphatase network will generate both main and complementary responses (Figure 1A). Gene ontology and protein-protein interaction analysis of all dynamic phosphoproteins revealed significant enrichment for main

HOG responses such as membrane ion transport channels but also complementary responses in morphogenesis and actin cytoskeleton dynamics (Figures 6A, 6B, S2, and S6; Data S2; Supplemental Results). There has been a renewed interest in the relationship between hydrodynamic pressure, cytoskeletal and mitotic spindle dynamics, and cellular and subcellular morphogenesis (Chowdhury et al., 1992; Kondo and Hayashi, 2013; Lancaster et al., 2013; Reiter et al., 2012; Stewart et al., 2011). The observed changes of phosphorylation in our study could thus provide a unique window onto early regulation of these processes.

Actin Structures and Microtubule Mobility Are Regulated by HOG

To explore effects of osmotic shock on F-actin, microtubule polymers, and clathrin-mediated endocytosis (CME), we integrated fluorescent-protein-coding oligonucleotides 3′ to reporter protein open reading frames in the genome by homologous recombination (Supplemental Experimental Procedures). We generated reporters to monitor in vivo behavior of actin cytoskeleton and cortical patches (actin-binding protein Abp1 and Abp140, cytoskeletal assembly protein Sla1, and F-Bar protein Syp1) and mitotic spindle (alpha-tubulin protein Tub1; Figures 6C–6F). Structural integrity of patches, actin cables, and spindles were not affected by salt treatment, but the monitored structures remained immobile for an unusually long time (Figures 6C–6F; Movies S1 and S2). The treatment also perturbed the normal maturation cycles of cortical patches, where Sla1 and Abp1 markers failed to progress with time and remained associated with patches at the plasma membrane instead of entering the cell (Figure 6C). We observed extensive phosphorylation changes in a number of proteins involved in different stages of endosome maturation including regulators of F-actin assembly (actin-binding proteins Ysc84 and Abp1) and Arp2/3-dependent branching (WASP homolog Las17, WASP-binding protein Lsb3, and verprolin Vrp1; Michelot et al., 2013; Table S2). It would be interesting to investigate whether these multi-target modifications result in complete inhibition of the endocytic cycle and block deleterious effects of cargo uptake, perhaps of the osmolytes themselves.

Dynamic Phosphoproteomic Analysis Provides Functional Insights into Polarization

To further investigate the functional predictive power of dynamic phosphoproteomics, we chose to study two regulated phosphosites on the F-Bar protein Syp1 (Figure 7A). In our competition-growth assay, only phospho-null mutants Syp1 S405A showed a fitness effect (Figures S5A and S5B). Both residues are located in the middle domain of Syp1. Ser405 is in a region necessary for polarized localization of Syp1 to bud tips (aa 365–565), and Ser347 is located within a region that is required for Syp1 plasma membrane (PM) localization (aa 300–365; Reider et al., 2009). We had previously proposed that Syp1 is central to a network linking cytoskeletal dynamics, endocytosis, monitoring of septin structure, and regulation of cell polarity and morphogenesis (Qiu et al., 2008; Stimpson et al., 2009; Tarassov et al., 2008). To determine whether these phosphosites could be implicated in localization and function of Syp1, we created phosphomimetic (serine to glutamic acid) or phospho-null mutants of Ser347 and Ser405 as GFP fusions and integrated their coding sequences into the genome by homologous recombination or expressed them from plasmids (Supplemental Experimental Procedures).

Overexpression (OE) of both Syp1 S347A and S347E were not elongated, and S347E cells were more circular than wild-type cells despite high expression levels (Figures 7B, 7C, and S7A). Fluorescently labeled Syp1 S347A displayed the normal punctate localization of Syp1 at the PM, whereas S347E was more diffusely distributed throughout the PM, suggesting that dephosphorylation of S347 is required for Syp1 localization to cortical patches (Figure 7B; Reider et al., 2009). This was in contrast to the polarized elongated phenotype caused simply by OE Syp1 (Qiu et al., 2008). OE Syp1 S405A also induced an elongated phenotype similar to OE Syp1 and appeared to be normally localized to cortical punctae (Figures 7C and S7B). In contrast, the OE Syp1 S405E mutant was not elongated but larger than wild-type cells and appeared localized into PM-associated punctae of larger bodies (Figures 7B, 7C, S7A, and S7B). It is important to note that S405E was significantly less expressed than wild-type Syp1 ($p < 10^{-16}$; Figure S7A). These results suggest that Ser347 must be dephosphorylated for Syp1 to localize to cortical patches, but localization is not sufficient to induce polarization. If, however, Ser405 is also dephosphorylated, polarization is induced (Figure 7D). Ser347 could also play a Ser405-independent role in polarization because both phosphomimetic and phospho-null OE mutants were not hyper-polarized.

Finally, because endocytic trafficking controls both symmetrical and asymmetric cell growth, we examined the effects of the Syp1 mutants on CME function with our Sla1 and Abp1 markers. The most-profound polarization was observed when we overexpressed Syp1 S405A in wild-type cells (*SYP1* locus is intact; Figures 7C and 7E). We also observed polarized endocytic patches at the growing tips of these cells but normal patch movement (Figure 7E). Taken together, our results suggest that dephosphorylation of Syp1 at residues Ser347 and Ser405 functions in the polarization of cell growth, in part through polarization of CME.

DISCUSSION

The motivation for studying dynamics of cellular processes has always been driven by the intuitive notion that specific and functionally relevant post-translational modifications should be dynamic in response to external or internal changes of state (Ideker and Krogan, 2012). This notion has motivated and driven the analysis of dynamic phosphoproteomes (Lynch, 2007; Olsen et al., 2006; Ong et al., 2002; Ong and Mann, 2006). However, we still do not know why only such a small proportion of observed phosphosites are dynamic and whether dynamic phosphosites are more likely functional.

We started from the general assumption that signaling networks have evolved so that kinase- or phosphatase-substrate interactions are made most efficient by the optimization of enzyme binding and specificity for substrate-recognition sequences (Bhattacharyya et al., 2006; Scott and Pawson, 2009; Zheng et al., 2013). We argued that, with such an organization, we would predict that early signaling events (phosphorylation or

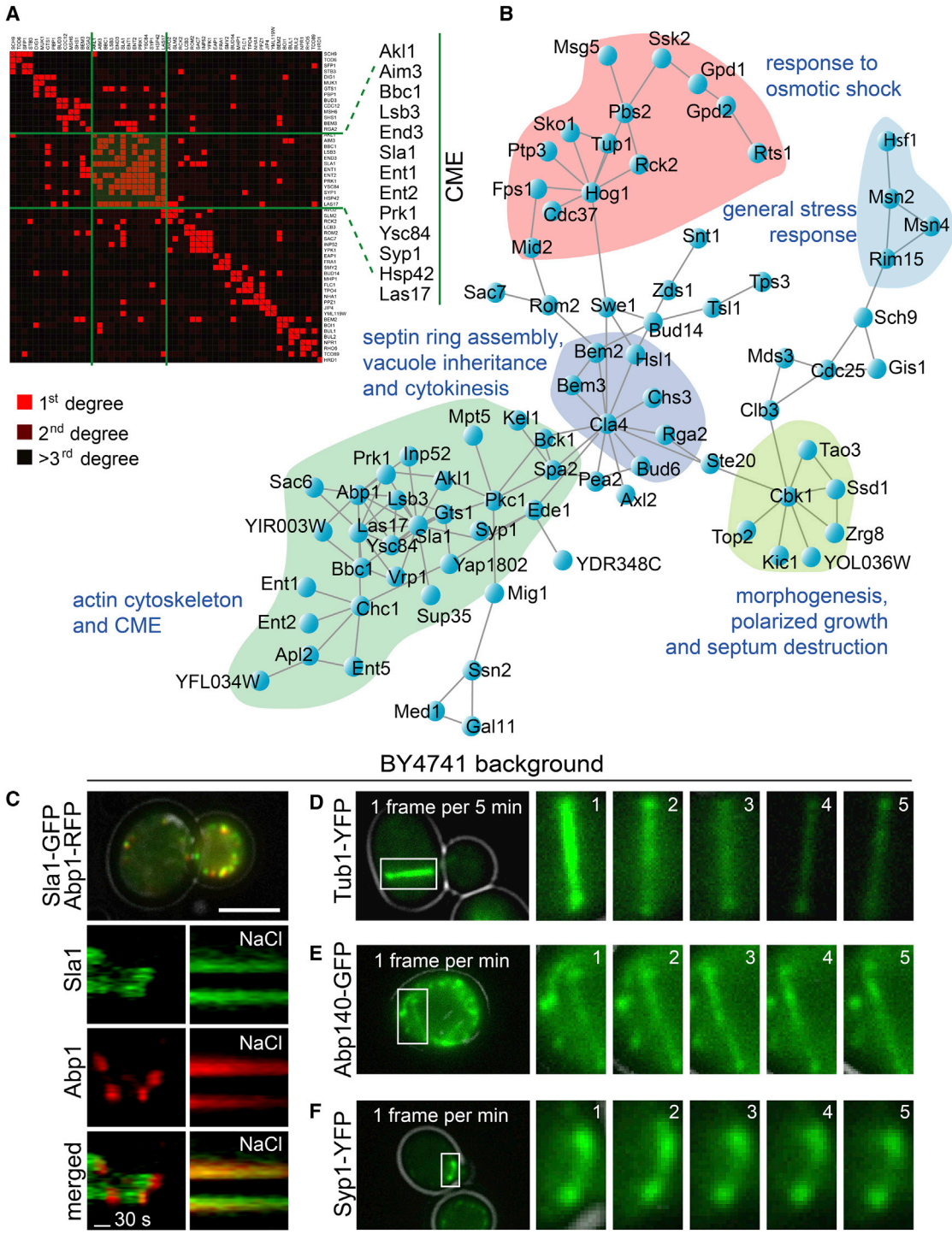

Figure 6. Dynamic Phosphosite Proteins Are Enriched for Both Main HOG and Complementary Responses

(A) Proteins with dynamic phosphorylation sites were used to cluster protein-protein interaction data from BioGrid. Green square shows proteins involved in clathrin-mediated endocytosis (CME).

(B) Protein interaction network for different GO terms (confidence >0.9 based on experimental data).

(C–F) We performed time-lapse fluorescent imaging of tubulin and actin structures in BY4741 cells treated with 0.4 M NaCl. (C) Cortical patches were monitored with Sla1-GFP and Abp1-mCherry at a rate of one frame per 5 s. The impact of salt is represented with kymographs for a time period of 3 min. (D) We observed reduced mobility of spindle microtubules with Tub1-Venus YFP, (E) actin cables and patches with Abp140-GFP, and (F) cortical patches and bud neck ring with Syp1-Venus YFP. Temporal changes of these structures under salt treatment are shown in the right panels at distinct frame frequencies. Scale bar represents 3 μm. See also Figure S6, Data S2, and Movies S1 and S2.

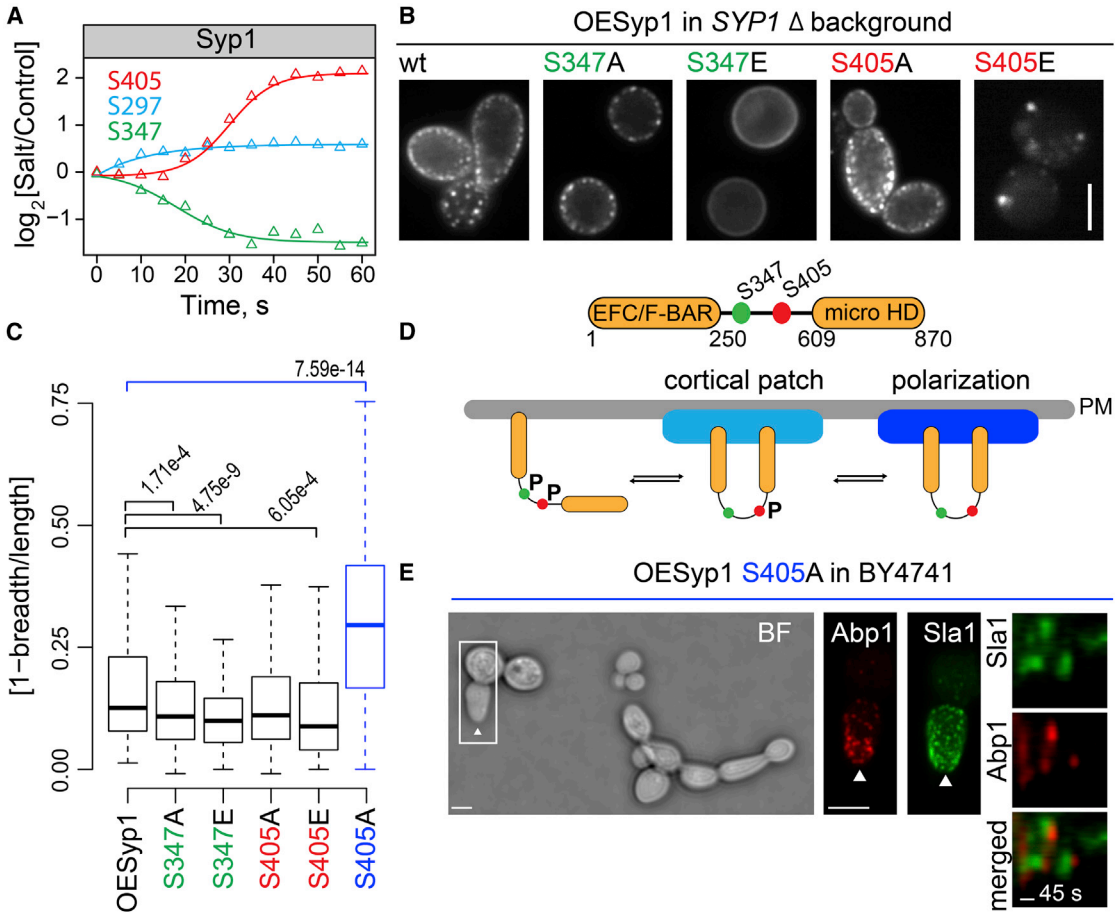

Figure 7. Syp1 Dynamic Phosphosites Are Involved in Regulation of Morphogenesis

(A) Three dynamic phosphosites on Syp1 may be implicated in control of polarization and cell growth.

(B) We generated phosphomimetic or phospho-null mutants of the Ser347 and Ser405 residues and assessed cell morphology and Syp1 localization of over-expressed (OE) Syp1 mutants in *SYP1*Δ deletion background. Scale bar represents 3 μm.

(C) We determined by morphometric analysis of segmented cells the elongation factor (one minus breadth/length) for OESyp1 (n = 293 cells) and S347A (n = 463 cells), S347E (n = 264 cells), S405A (n = 493 cells), and S405E (n = 209 cells) mutant strains in *SYP1* deletion background (black boxplots) and also for OESyp1 S405A (n = 438 cells) in the wild-type background (blue boxplot). Student's t tests were performed to compare a sampling of 200 cells from OESyp1 to all other strains; p values are indicated if <0.05.

(D) Syp1 was proposed to contain two main domains separated by a flexible middle region from residues 250 to 609. This middle region contains both dynamic phosphosites S347 and S405. In vivo N-terminal EFC/F-Bar domain is believed to act in Syp1 plasma membrane (PM) association, and the C-terminal microHD domain is necessary for Syp1 interaction with endocytic adaptor Ede1. Syp1 is central to a network linking cytoskeletal dynamics, endocytosis, monitoring of septin structure, and regulation of cell polarity. We propose that cortical patch localization of Syp1 requires S347 dephosphorylation whereas Syp1 function in cell polarization is regulated by S405 phosphorylation.

(E) We assessed the OESyp1 S405A elongated cell phenotype, its impact on endocytosis by microscopy (bright-field and fluorescent images), and behavior of cortical patch fluorescent markers Sla1-GFP and Abp1-mCherry in S405A mutant cells (left and middle). Scale bar represents 2 μm. The behavior of cortical patches in the S405A strain (wild-type background) was monitored as described above and is represented with kymographs for a time period of 5 min (right).

See also Figure S7.

dephosphorylation) are most likely functional, but slower phosphorylated sites could represent promiscuous phosphorylation that have no functional consequences (Landry et al., 2009; Levy et al., 2012).

We found the HOG response to be complex, integrating a large proportion of the kinases and phosphatases in the cell and initiating a large number of changes in protein phosphorylation. Based on the conservation of these dynamically modulated sites, they are likely enriched in specific and functional sites, but promiscuous phosphorylation must also be occurring over longer timescales, reflected in the lower average conservation of static phosphosites. It is important, however, to note that static sites are not necessarily non-functional. They may be dynamic and have functions under other conditions or in different time frames following osmotic shock.

Thus, the HOG-signaling network appears to have evolved so that promiscuous phosphorylation is slower to appear than functional phosphorylation. The lower conservation of static

phosphosites suggests that they may be the result of promiscuous phosphorylation that accumulate and persist over more than one cell cycle.

Although functional phosphosites represent a small subset of the phosphoproteome, optimizing specificity in signaling networks may come at a higher cost to the cell than the occurrence of some promiscuous phosphorylation. There may also be a tradeoff between the rate at which kinases and phosphatases act on their substrates and the specificity of kinase- and phosphatase-substrate interactions. Optimization of either could reduce the other, and thus, cells may have evolved to achieve the best possible specificity at limited cost (Levy et al., 2012; Tawfik, 2010).

Two final points must be stressed about the interpretation of phosphosite conservation. First, dynamic or static phosphosites that are weakly conserved are not necessarily non-functional but may simply reflect functional sites that have been evolving rapidly. Second, the evolution of transcriptional regulatory networks can be both rapid and extensive and so can protein regulatory networks, such as kinase-phosphatase networks. The evolution of such networks can contribute to both intra- and inter-species diversification, and promiscuous phosphorylation may be one mechanism by which signaling networks evolve (Moses and Landry, 2010).

We observed a narrow range of kinetic rates for dynamic profiles that may reflect the physical organization of signaling networks and relative abundances of enzymes and their substrates. One condition under which homogeneous rates might be observed would be if the kinase or phosphatase reactions occur at saturation due to their high abundances compared to substrates. It has in fact been noted recently that kinases or phosphatases are indeed often more abundant than their substrates (Martins and Swain, 2011). In addition, kinases and phosphatases can form complexes with their substrates, either directly or through scaffold or adaptor proteins (Bhattacharyya et al., 2006; Scott and Pawson, 2009; Zheng et al., 2013). In both cases, maximum efficiency of reactions can be achieved.

Finally, the accurate prediction of functional versus non-functional post-translational modifications remains a significant challenge. The strategy we describe here is based on the general idea that good predictions of functionality could be derived based on chemical principles of molecular interactions (Landry, 2011; Landry et al., 2013). The strategy can be applied to other signaling responses and post-translational modifications and may reveal a deeper understanding of the evolution and organization of signaling machineries. In addition, combining information about the conservation of the post-translational modifications with careful analysis of the proportion of a protein that is dynamically phosphorylated may provide the best possible predictions of phosphosite functionality (Levy et al., 2012; Wu et al., 2011).

EXPERIMENTAL PROCEDURES

Cell Treatment and Protein Extraction

*LYS1*Δ::kanMX; *ARG4*Δ::kanMX strain was grown in synthetic dextrose supplemented with either ^{12}C-, ^{14}N- (light) or ^{13}C-, ^{15}N- (heavy) lysine and arginine. Heavy cultures were treated with 4 M NaCl dissolved in the culture medium to a final concentration of 0.4 M NaCl. In order to stop all metabolic activity at specific times, individual light and heavy cultures were combined at fixed interval following treatment (0–60 s at 5 s intervals) in liquid nitrogen. Cells were lysed by mechanical grinding under liquid nitrogen, and proteins were precipitated with TCA.

Phosphopeptide Isolation and Offline Fractionation

Tryptic digest samples were subjected to a TiO_2 enrichment protocol. Briefly, sample loading, washing, and elution steps were performed in homemade spin columns assembled following the StageTip extraction (Ishihama et al., 2006; Kanshin et al., 2013; Rappsilber et al., 2003). In order to increase phosphoproteome coverage prior to MS analysis, phosphopeptides were fractionated offline by SCX chromatography.

nanoLC-MS/MS and Data Processing

SCX fractions obtained after offline fractionation were analyzed by online reverse-phase chromatography with a nanoflow HPLC system coupled with an electrospray ionization interface to acquire MS and MS/MS scans. Peptides were analyzed using an automated data-dependent acquisition on a LTQ-Orbitrap Elite mass spectrometer. MS data were analyzed using MaxQuant (Cox and Mann, 2008; Cox et al., 2011b) software version 1.3.0.3. The precursor mass tolerance was set to 20 ppm for the first search (used for non-linear mass re-calibration; Cox et al., 2011a) and then to 6 ppm for the main search. The FDR for peptide, protein, and site identification was set to 1%.

Data Filtering and Significance

We considered only peptides for which isotopic abundance ratios (fold change = salt/control) were measured in at least ten time points (out of 13), and we set a cutoff for phosphosite localization confidence across experiments (time points) to 0.75. Based on these criteria, we obtained 5,453 high-confidence phosphosite kinetic profiles (Table S1). We used both fold-change-based and pattern-based analyses to obtain a list of 596 regulated profiles (Table S2) defined as dynamic phosphopeptides.

Site-Directed Mutagenesis, Competition-Growth Assays, and Microscopy

Plasmid construction, cloning, and gene manipulations were performed using standard methods. For the competition growth assays, mutant and wild-type starter cultures were mixed in equal quantities, diluted 1:100, and grown in competition in exponential growth phase at 30°C for 5 days in normal LFM or LFM supplemented with 1 M NaCl. We measured corresponding population fractions every 8 hr as determined by fluorescence spectroscopy with a Gemini XS microplate reader. Images for Figures 6 and 7 were collected with either a Nikon TE2000 inverted microscope or an InCell 6000 automated confocal microscope. Detailed experimental, modeling, and analysis methods are described in Supplemental Experimental Procedures.

SUPPLEMENTAL INFORMATION

Supplemental Information includes Supplemental Results, Supplemental Experimental Procedures, seven figures, three tables, two movies, and two data files and can be found with this article online at http://dx.doi.org/10.1016/j.celrep.2015.01.052.

AUTHOR CONTRIBUTIONS

E.K., L.-P.B.-S., P.T., and S.W.M. designed research; E.K. and L.-P.B.-S. contributed equally to this work and performed research; E.K., L.-P.B.-S., S.S.I., P.T., and S.W.M. analyzed data; and E.K., L.-P.B.-S., P.T., and S.W.M. wrote the paper.

ACKNOWLEDGMENTS

The authors thank Jacqueline Kowarzyk for invaluable assistance and advice for growth-competition assays, Jackie Vogel (McGill University) for reagents and critical comments and advice on the manuscript, Ole Jensen (University of Southern Denmark) for strains, and Thomas Pollard (Yale University) and David Drubin (University of California, Berkeley) for critical comments and

advice on the manuscript. The authors acknowledge support from CIHR grants MOP-GMX-152556 (to S.W.M.), MOP-GMX-231013 (to S.W.M. and P.T.), and NSERC grant 311598 (to P.T.). The Institute for Research in Immunology and Cancer (IRIC) receives infrastructure support from the Canadian Center of Excellence in Commercialization and Research, the Canadian Foundation for Innovation, and the Fonds de Recherche du Québec - Santé (FRQS).

Received: January 21, 2014
Revised: December 22, 2014
Accepted: January 20, 2015
Published: February 19, 2015

REFERENCES

Bettinger, B.T., Clark, M.G., and Amberg, D.C. (2007). Requirement for the polarisome and formin function in Ssk2p-mediated actin recovery from osmotic stress in Saccharomyces cerevisiae. Genetics *175*, 1637–1648.

Bhattacharyya, R.P., Reményi, A., Yeh, B.J., and Lim, W.A. (2006). Domains, motifs, and scaffolds: the role of modular interactions in the evolution and wiring of cell signaling circuits. Annu. Rev. Biochem. *75*, 655–680.

Bilsland-Marchesan, E., Ariño, J., Saito, H., Sunnerhagen, P., and Posas, F. (2000). Rck2 kinase is a substrate for the osmotic stress-activated mitogen-activated protein kinase Hog1. Mol. Cell. Biol. *20*, 3887–3895.

Bodenmiller, B., Wanka, S., Kraft, C., Urban, J., Campbell, D., Pedrioli, P.G., Gerrits, B., Picotti, P., Lam, H., Vitek, O., et al. (2010). Phosphoproteomic analysis reveals interconnected system-wide responses to perturbations of kinases and phosphatases in yeast. Sci. Signal. *3*, rs4.

Breitkreutz, A., Choi, H., Sharom, J.R., Boucher, L., Neduva, V., Larsen, B., Lin, Z.Y., Breitkreutz, B.J., Stark, C., Liu, G., et al. (2010). A global protein kinase and phosphatase interaction network in yeast. Science *328*, 1043–1046.

Chen, R.E., and Thorner, J. (2007). Function and regulation in MAPK signaling pathways: lessons learned from the yeast Saccharomyces cerevisiae. Biochim. Biophys. Acta *1773*, 1311–1340.

Chou, M.F., and Schwartz, D. (2011). Biological sequence motif discovery using motif-x. Curr. Protoc. Bioinformatics *Chapter 13*, 15–24.

Chowdhury, S., Smith, K.W., and Gustin, M.C. (1992). Osmotic stress and the yeast cytoskeleton: phenotype-specific suppression of an actin mutation. J. Cell Biol. *118*, 561–571.

Cox, J., and Mann, M. (2008). MaxQuant enables high peptide identification rates, individualized p.p.b.-range mass accuracies and proteome-wide protein quantification. Nat. Biotechnol. *26*, 1367–1372.

Cox, J., Michalski, A., and Mann, M. (2011a). Software lock mass by two-dimensional minimization of peptide mass errors. J. Am. Soc. Mass Spectrom. *22*, 1373–1380.

Cox, J., Neuhauser, N., Michalski, A., Scheltema, R.A., Olsen, J.V., and Mann, M. (2011b). Andromeda: a peptide search engine integrated into the MaxQuant environment. J. Proteome Res. *10*, 1794–1805.

Gustin, M.C., Albertyn, J., Alexander, M., and Davenport, K. (1998). MAP kinase pathways in the yeast Saccharomyces cerevisiae. Microbiol. Mol. Biol. Rev. *62*, 1264–1300.

Harsha, H.C., Molina, H., and Pandey, A. (2008). Quantitative proteomics using stable isotope labeling with amino acids in cell culture. Nat. Protoc. *3*, 505–516.

Hersen, P., McClean, M.N., Mahadevan, L., and Ramanathan, S. (2008). Signal processing by the HOG MAP kinase pathway. Proc. Natl. Acad. Sci. USA *105*, 7165–7170.

Ho, C.H., Magtanong, L., Barker, S.L., Gresham, D., Nishimura, S., Natarajan, P., Koh, J.L., Porter, J., Gray, C.A., Andersen, R.J., et al. (2009). A molecular barcoded yeast ORF library enables mode-of-action analysis of bioactive compounds. Nat. Biotechnol. *27*, 369–377.

Ideker, T., and Krogan, N.J. (2012). Differential network biology. Mol. Syst. Biol. *8*, 565.

Ishihama, Y., Rappsilber, J., and Mann, M. (2006). Modular stop and go extraction tips with stacked disks for parallel and multidimensional Peptide fractionation in proteomics. J. Proteome Res. *5*, 988–994.

Kanshin, E., Michnick, S.W., and Thibault, P. (2013). Displacement of N/Q-rich peptides on TiO2 beads enhances the depth and coverage of yeast phosphoproteome analyses. J. Proteome Res. *12*, 2905–2913.

Kondo, T., and Hayashi, S. (2013). Mitotic cell rounding accelerates epithelial invagination. Nature *494*, 125–129.

Lancaster, O.M., Le Berre, M., Dimitracopoulos, A., Bonazzi, D., Zlotek-Zlotkiewicz, E., Picone, R., Duke, T., Piel, M., and Baum, B. (2013). Mitotic rounding alters cell geometry to ensure efficient bipolar spindle formation. Dev. Cell *25*, 270–283.

Landry, C.R. (2011). Cell biology. A cellular roadmap for the plant kingdom. Science *333*, 532–533.

Landry, C.R., Levy, E.D., and Michnick, S.W. (2009). Weak functional constraints on phosphoproteomes. Trends Genet. *25*, 193–197.

Landry, C.R., Levy, E.D., Abd Rabbo, D., Tarassov, K., and Michnick, S.W. (2013). Extracting insight from noisy cellular networks. Cell *155*, 983–989.

Lee, Y.J., Jeschke, G.R., Roelants, F.M., Thorner, J., and Turk, B.E. (2012). Reciprocal phosphorylation of yeast glycerol-3-phosphate dehydrogenases in adaptation to distinct types of stress. Mol. Cell. Biol. *32*, 4705–4717.

Lee, J., Reiter, W., Dohnal, I., Gregori, C., Beese-Sims, S., Kuchler, K., Ammerer, G., and Levin, D.E. (2013). MAPK Hog1 closes the S. cerevisiae glycerol channel Fps1 by phosphorylating and displacing its positive regulators. Genes Dev. *27*, 2590–2601.

Levy, E.D., Landry, C.R., and Michnick, S.W. (2010). Cell signaling. Signaling through cooperation. Science *328*, 983–984.

Levy, E.D., Michnick, S.W., and Landry, C.R. (2012). Protein abundance is key to distinguish promiscuous from functional phosphorylation based on evolutionary information. Philos. Trans. R. Soc. Lond. B Biol. Sci. *367*, 2594–2606.

Linding, R., Jensen, L.J., Ostheimer, G.J., van Vugt, M.A., Jørgensen, C., Miron, I.M., Diella, F., Colwill, K., Taylor, L., Elder, K., et al. (2007). Systematic discovery of in vivo phosphorylation networks. Cell *129*, 1415–1426.

Lynch, M. (2007). The evolution of genetic networks by non-adaptive processes. Nat. Rev. Genet. *8*, 803–813.

Macia, J., Regot, S., Peeters, T., Conde, N., Solé, R., and Posas, F. (2009). Dynamic signaling in the Hog1 MAPK pathway relies on high basal signal transduction. Sci. Signal. *2*, ra13.

Manning, G., Plowman, G.D., Hunter, T., and Sudarsanam, S. (2002). Evolution of protein kinase signaling from yeast to man. Trends Biochem. Sci. *27*, 514–520.

Martins, B.M., and Swain, P.S. (2011). Trade-offs and constraints in allosteric sensing. PLoS Comput. Biol. *7*, e1002261.

Mattison, C.P., and Ota, I.M. (2000). Two protein tyrosine phosphatases, Ptp2 and Ptp3, modulate the subcellular localization of the Hog1 MAP kinase in yeast. Genes Dev. *14*, 1229–1235.

Michelot, A., Grassart, A., Okreglak, V., Costanzo, M., Boone, C., and Drubin, D.G. (2013). Actin filament elongation in Arp2/3-derived networks is controlled by three distinct mechanisms. Dev. Cell *24*, 182–195.

Mok, J., Kim, P.M., Lam, H.Y., Piccirillo, S., Zhou, X., Jeschke, G.R., Sheridan, D.L., Parker, S.A., Desai, V., Jwa, M., et al. (2010). Deciphering protein kinase specificity through large-scale analysis of yeast phosphorylation site motifs. Sci. Signal. *3*, ra12.

Moses, A.M., and Landry, C.R. (2010). Moving from transcriptional to phospho-evolution: generalizing regulatory evolution? Trends Genet. *26*, 462–467.

Muzzey, D., Gómez-Uribe, C.A., Mettetal, J.T., and van Oudenaarden, A. (2009). A systems-level analysis of perfect adaptation in yeast osmoregulation. Cell *138*, 160–171.

Nguyen Ba, A.N., and Moses, A.M. (2010). Evolution of characterized phosphorylation sites in budding yeast. Mol. Biol. Evol. *27*, 2027–2037.

Olsen, J.V., Blagoev, B., Gnad, F., Macek, B., Kumar, C., Mortensen, P., and Mann, M. (2006). Global, in vivo, and site-specific phosphorylation dynamics in signaling networks. Cell *127*, 635–648.

Ong, S.E., and Mann, M. (2006). A practical recipe for stable isotope labeling by amino acids in cell culture (SILAC). Nat. Protoc. *1*, 2650–2660.

Ong, S.E., Blagoev, B., Kratchmarova, I., Kristensen, D.B., Steen, H., Pandey, A., and Mann, M. (2002). Stable isotope labeling by amino acids in cell culture, SILAC, as a simple and accurate approach to expression proteomics. Mol. Cell. Proteomics *1*, 376–386.

Proft, M., and Struhl, K. (2002). Hog1 kinase converts the Sko1-Cyc8-Tup1 repressor complex into an activator that recruits SAGA and SWI/SNF in response to osmotic stress. Mol. Cell *9*, 1307–1317.

Qiu, W., Neo, S.P., Yu, X., and Cai, M. (2008). A novel septin-associated protein, Syp1p, is required for normal cell cycle-dependent septin cytoskeleton dynamics in yeast. Genetics *180*, 1445–1457.

Rappsilber, J., Ishihama, Y., and Mann, M. (2003). Stop and go extraction tips for matrix-assisted laser desorption/ionization, nanoelectrospray, and LC/MS sample pretreatment in proteomics. Anal. Chem. *75*, 663–670.

Reider, A., Barker, S.L., Mishra, S.K., Im, Y.J., Maldonado-Báez, L., Hurley, J.H., Traub, L.M., and Wendland, B. (2009). Syp1 is a conserved endocytic adaptor that contains domains involved in cargo selection and membrane tubulation. EMBO J. *28*, 3103–3116.

Reiser, V., Ruis, H., and Ammerer, G. (1999). Kinase activity-dependent nuclear export opposes stress-induced nuclear accumulation and retention of Hog1 mitogen-activated protein kinase in the budding yeast Saccharomyces cerevisiae. Mol. Biol. Cell *10*, 1147–1161.

Reiter, W., Anrather, D., Dohnal, I., Pichler, P., Veis, J., Grøtli, M., Posas, F., and Ammerer, G. (2012). Validation of regulated protein phosphorylation events in yeast by quantitative mass spectrometry analysis of purified proteins. Proteomics *12*, 3030–3043.

Reiter, W., Klopf, E., De Wever, V., Anrather, D., Petryshyn, A., Roetzer, A., Niederacher, G., Roitinger, E., Dohnal, I., Görner, W., et al. (2013). Yeast protein phosphatase 2A-Cdc55 regulates the transcriptional response to hyperosmolarity stress by regulating Msn2 and Msn4 chromatin recruitment. Mol. Cell. Biol. *33*, 1057–1072.

Rep, M., Reiser, V., Gartner, U., Thevelein, J.M., Hohmann, S., Ammerer, G., and Ruis, H. (1999). Osmotic stress-induced gene expression in Saccharomyces cerevisiae requires Msn1p and the novel nuclear factor Hot1p. Mol. Cell. Biol. *19*, 5474–5485.

Saito, H., and Posas, F. (2012). Response to hyperosmotic stress. Genetics *192*, 289–318.

Schwartz, D., and Gygi, S.P. (2005). An iterative statistical approach to the identification of protein phosphorylation motifs from large-scale data sets. Nat. Biotechnol. *23*, 1391–1398.

Scott, J.D., and Pawson, T. (2009). Cell signaling in space and time: where proteins come together and when they're apart. Science *326*, 1220–1224.

Sharrocks, A.D., Yang, S.H., and Galanis, A. (2000). Docking domains and substrate-specificity determination for MAP kinases. Trends Biochem. Sci. *25*, 448–453.

Soufi, B., Kelstrup, C.D., Stoehr, G., Fröhlich, F., Walther, T.C., and Olsen, J.V. (2009). Global analysis of the yeast osmotic stress response by quantitative proteomics. Mol. Biosyst. *5*, 1337–1346.

Stewart, M.P., Helenius, J., Toyoda, Y., Ramanathan, S.P., Muller, D.J., and Hyman, A.A. (2011). Hydrostatic pressure and the actomyosin cortex drive mitotic cell rounding. Nature *469*, 226–230.

Stimpson, H.E., Toret, C.P., Cheng, A.T., Pauly, B.S., and Drubin, D.G. (2009). Early-arriving Syp1p and Ede1p function in endocytic site placement and formation in budding yeast. Mol. Biol. Cell *20*, 4640–4651.

Tarassov, K., Messier, V., Landry, C.R., Radinovic, S., Serna Molina, M.M., Shames, I., Malitskaya, Y., Vogel, J., Bussey, H., and Michnick, S.W. (2008). An in vivo map of the yeast protein interactome. Science *320*, 1465–1470.

Tawfik, D.S. (2010). Messy biology and the origins of evolutionary innovations. Nat. Chem. Biol. *6*, 692–696.

Tay, S., Hughey, J.J., Lee, T.K., Lipniacki, T., Quake, S.R., and Covert, M.W. (2010). Single-cell NF-kappaB dynamics reveal digital activation and analogue information processing. Nature *466*, 267–271.

Teige, M., Scheikl, E., Reiser, V., Ruis, H., and Ammerer, G. (2001). Rck2, a member of the calmodulin-protein kinase family, links protein synthesis to high osmolarity MAP kinase signaling in budding yeast. Proc. Natl. Acad. Sci. USA *98*, 5625–5630.

Vaga, S., Bernardo-Faura, M., Cokelaer, T., Maiolica, A., Barnes, C.A., Gillet, L.C., Hegemann, B., van Drogen, F., Sharifian, H., Klipp, E., et al. (2014). Phosphoproteomic analyses reveal novel cross-modulation mechanisms between two signaling pathways in yeast. Mol. Syst. Biol. *10*, 767.

Willbrand, K., Radvanyi, F., Nadal, J.P., Thiery, J.P., and Fink, T.M. (2005). Identifying genes from up-down properties of microarray expression series. Bioinformatics *21*, 3859–3864.

Wu, R., Haas, W., Dephoure, N., Huttlin, E.L., Zhai, B., Sowa, M.E., and Gygi, S.P. (2011). A large-scale method to measure absolute protein phosphorylation stoichiometries. Nat. Methods *8*, 677–683.

Yuzyuk, T., and Amberg, D.C. (2003). Actin recovery and bud emergence in osmotically stressed cells requires the conserved actin interacting mitogen-activated protein kinase kinase kinase Ssk2p/MTK1 and the scaffold protein Spa2p. Mol. Biol. Cell *14*, 3013–3026.

Yuzyuk, T., Foehr, M., and Amberg, D.C. (2002). The MEK kinase Ssk2p promotes actin cytoskeleton recovery after osmotic stress. Mol. Biol. Cell *13*, 2869–2880.

Zheng, Y., Zhang, C., Croucher, D.R., Soliman, M.A., St-Denis, N., Pasculescu, A., Taylor, L., Tate, S.A., Hardy, W.R., Colwill, K., et al. (2013). Temporal regulation of EGF signalling networks by the scaffold protein Shc1. Nature *499*, 166–171.